HHS Public Access

Author manuscript

New J Chem. Author manuscript; available in PMC 2019 September 07.

Published in final edited form as:

New J Chem. 2018 September 7; 42(17): 14551–14558. doi:10.1039/C8NJ03067G.

New thiophene-based C_{60} fullerene derivatives as efficient electron transporting materials for perovskite solar cells

Edison Castro[a,*], **Olivia Fernandez-Delgado**[a], **Funda Arslan**[a], **Gerardo Zavala**[a], **Tingyuan Yang**[a], **Sairaman Seetharaman**[b], **Francis D' Souza**[b], and **Luis Echegoyen**[a,*]

[a]Department of Chemistry, University of Texas at El Paso, 500 West University Avenue, El Paso, TX 79968, United States

[b]Department of Chemistry, University of North Texas Denton, TX 76203-5017, United States

Abstract

The synthesis of new C_{60} fullerene derivatives functionalized with thiophene moieties as well as with electron donating or electron withdrawing groups, bromine (Br) or cyano (CN), respectively, using Bingel reactions is reported. The synthesized derivatives were used as the electron transporting materials (ETMs) in inverted perovskite solar cells (PSCs). Compared to devices fabricated with [6,6]-phenyl-C_{61}-butyric acid methyl ester ($PC_{61}BM$), the new derivatives showed similar electrochemical properties and electron mobilities. However, PSCs based on the new derivatives synthesized in this work exhibited higher power conversion efficiencies (PCEs) than $PC_{61}BM$ based devices, which were ascribed to their better passivation ability, likely due to specific interactions between the fullerene addend and the perovskite layer surface. Devices based on the fullerene bearing the CN group exhibited an additionally improved efficiency due to the increased dielectric constant (ε_r) of this derivative. These results show that the new functionalized fullerene derivatives can act as efficient ETMs in inverted PSCs.

TOC

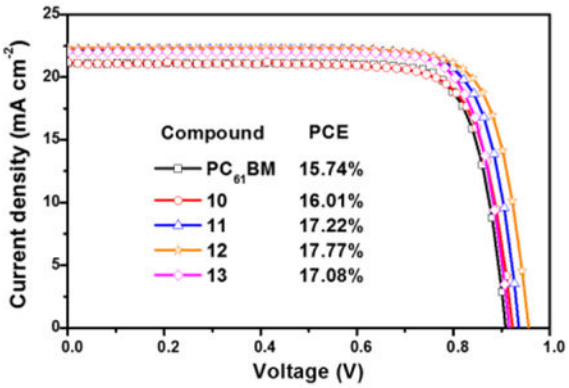

Correspondence to: Edison Castro; Olivia Fernandez-Delgado.

[*]**Corresponding author**, eacastroportillo@utep.edu, echegoyen@utep.edu.

Conflict of interest

There are no conflicts to declare.

Devices based on the new fullerene derivatives exhibited an improved overall performance compared to those with $PC_{61}BM$ as the electron transporting material.

Keywords

fullerene derivatives; thiophene; Bingel adducts; electron transporting materials; perovskite solar cells

Introduction

In the past few years the development of organic-inorganic hybrid PSCs has progressed quickly not only because of their increasing PCE values (certified values up to 22.7%)[1] but also because of their multiple applications.[2–5] To find more viable and efficient PSC device-configurations, the inverted structures are very promising due to their easy fabrication[6, 7] and relatively high PCEs (21.0%, highest certified value),[8] among other reasons. Inverted structures are typically fabricated using a transparent indium tin oxide electrode or fluorinated tin oxide (ITO or FTO, respectively),[9, 10] a hole transporting layer (HTL) of poly(3,4-ethylenedioxythiophene)-poly(styrenesulfonate) (PEDOT:PSS),[11] nickel oxide (NiO_x)[12] or poly[bis(4-phenyl)(2,4,6-trimethylphenyl)amine] (PTAA),[8] followed by the perovskite layer,[6] the electron transporting layer (ETL, mainly fullerenes),[6] and the back metal electrode (Al or Ag).[13, 14] The ETL not only extracts and transports the electrons from the perovskite layer to the back electrode, it also avoids water intrusion from the environment to the perovskite layer, thus retarding perovskite degradation.[13] In this regard, the relatively good electron mobility, solution processability, and HOMO/LUMO levels that match with those of the perovskite make fullerenes highly promising ETMs in inverted PSCs.[6, 15–17]

Besides $PC_{61}BM$, several fullerene derivatives have been used as the ETMs in PSCs.[6] In a first attempt to understand the role of the fullerenes' addend on PSCs, we studied the effect of amino and carboxylic groups on both C_{60} and C_{70} fullerene cages (dimethoxy carbonyl pyrrolidine $C_{60/70}$ $DMEC_{60}$ and $DMEC_{70}$, respectively), where some specific interactions between the perovskite and the amino and carboxyl groups were observed using FTIR,[10] which yielded improved device performances and long-term device stabilities, compared to $PC_{61}BM$-based devices.

One limitation of the PSCs is that the perovskite crystals contain uncoordinated ions at the crystal surface and at the grain boundaries,[18] which are electron trap sites that give rise to charge recombination and hysteretic behavior.[19] Passivation of these trap sites has become crucial to fabricate high performing PSCs. Noel *et al.* reported that organic Lewis bases such as thiophene and pyridine can passivate the crystal surfaces of the perovskite by coordination between the sulfur atom of the thiophene or the nitrogen atom of the pyridine with under-coordinated Pb^{+2} (Lewis acid) in the perovskite, resulting in PCE improvements up to 27%.[18] It has also been reported that fullerenes can passivate these trap states at the surface as well as at the grain boundaries, being extensively used to reduce/eliminate hysteretic behavior for both regular and inverted PSC configurations.[6, 15–17] By using time-resolved (TR) and steady state photoluminescence (PL), combined with impedance

spectroscopy measurements, Shao *et al.* reported that trap-assisted recombination at the perovskite/fullerene interface is effectively suppressed when using a fullerene derivative with a higher ε_r.[20] The most common approaches to increase the ε_r on fullerenes is by introducing highly polar groups such as CN[21] or triethyleneglycol (TEG).[22]

Considering the above-mentioned characteristics, and without sacrificing optical, electronic and solubility properties, here we report the synthesis of new C_{60} fullerene derivatives that contain thiophene- (Lewis base) and either a CN group (to increase ε_r) or Br, and their application as efficient ETMs in inverted PSCs. In all cases, PSCs based on the new fullerene derivatives exhibited improved overall performance and long-term device stability than those based on $PC_{61}BM$.

Materials Synthesis

Experimental

All chemicals were reagent grade. Silica gel (40–60 μ, 60 Å) was used to separate and purify the products. Matrix-assisted laser desorption/ionization time-of-flight mass spectroscopy (MALDI-TOF-MS) was conducted on positive mode, with samples dissolved in carbon disulfide and 1,1,4,4-tetraphenyl-1,3-butadiene (TPB) as matrix. NMR spectra were recorded using a Bruker 400 MHz spectrometer. The UV/Vis-NIR spectra were recorded for chloroform solutions. Cyclic voltammetry (CV) experiments were carried out under an argon atmosphere at room temperature. The scan rate for the CV experiments was 100 mV/s. A one compartment cell with a standard three-electrode set up was used, consisting of a 1 mm diameter glassy carbon disk as the working electrode, a platinum wire as the counter electrode and a silver wire as a pseudo-reference electrode, in a solution of anhydrous *o*-DCB containing 0.05 M *n*-Bu_4NPF_6. Ferrocene was added to the solution at the end of each experiment as an internal standard.

Synthesis of compound 6: Compound **1** (640 mg, 5 mmol) and compound **2** (755 mg, 5 mmol) were dissolved in dry THF (30 mL) and stirred for 5 min at room temperature. Triethylamine (TEA) (1 mL, 7.2 mmol) was added dropwise to the solution and the reaction mixture was stirred for 5 h at room temperature. The solvent was dried under vacuum and the crude product was purified by silica gel column chromatography using a mixture of hexanes:ethyl acetate (4:1 ratio). Compound **6** was obtained as a colorless oil; yield 85%.

Synthesis of compound 7: Compound **7** was synthesized following the same procedure as that used for the synthesis of compound **6**. The crude product was purified by silica gel column chromatography using a mixture of hexanes:ethyl acetate (9:1 ratio). Compound **7** was obtained as a colorless oil; yield 89%.

Synthesis of compound 8: To 805 mg (5 mmol) of compound **4** dissolved in dry dichloromethane (50 mL), 1545 mg (7.5 mmol) of dicyclohexylcarbodiimide (DCC) were added at room temperature. The reaction was stirred for 10 min and 2483 mg (7.5 mmol) of 4-dimethylaminopyridine (DMAP) were added and the reaction was stirred for 10 min. 640 mg (5 mmol) of compound **1** were added and the reaction was stirred overnight at room temperature. The mixture was filtered to remove the solid. The solvent was removed under

vacuum and the crude was purified by silica gel column chromatography using a mixture of hexanes:ethyl acetate (4:1 ratio). Compound **8** was obtained as a white solid; yield 93%.

Synthesis of compound 9: Compound **9** was synthesized following the same procedure than that used for the synthesis of compound **8**. The crude product was purified by silica gel column chromatography using a mixture of hexanes:ethyl acetate (9:1 ratio). Compound **9** was obtained as a colorless oil; yield 84%.

Synthesis of compound 10: C_{60} (72 mg, 0.1 mmol) was dissolved in *o*-DCB (15 mL) and compound **6** (30 mg, 0.12 mmol) and tetrabromomethane (CBr_4) (75 mg, 0.22 mmol) were added and stirred at room temperature for 2 min. 1,8-Diazabicyclo[5.4.0]undec-7-ene (DBU) (16 mg, 0.1 mmol) was added and the reaction was stirred for 10 minutes. After the addition of the DBU the reaction was monitored by thin layer chromatography (TLC) using CS_2 to check the unreacted C_{60} and a mixture of CS_2:$CHCl_3$ (4:1 ratio) to track the formation of the monoadduct derivative. The solution was directly poured onto a silica gel column and CS_2 was used to separate the non-reacted C_{60}. Compound **10** was purified using a CS_2:$CHCl_3$ (4:1) mixture, yield 59%.

Synthesis of compound 11: Compound **11** was synthesized following the same procedure as that used for the synthesis of compound **10**. Compound **11** was purified using a CS_2:$CHCl_3$ (4:1) mixture; yield 55%.

Synthesis of compound 12: Compound **12** was synthesized following the same procedure as that used for the synthesis of compound **10**. Compound **12** was purified using toluene; yield 56%.

Synthesis of compound 13: Compound **13** was synthesized following the same procedure as that used for the synthesis of compound **10**. Compound **13** was purified using CS_2:$CHCl_3$ (9:1) mixture; yield 54%.

Device Fabrication

$PC_{61}BM$ (99%) was bought from SES Research. Methylammonium iodide (CH_3NH_3I, 99.5%) was bought from Greatcellsolar. PbI_2 (99%) was bought from Sigma-Aldrich. The configuration used for the fabrication of the PSCs was ITO/PEDOT:PSS/ $CH_3NH_3PbI_3$/ETM/Al. The patterned ITO glass substrates were cleaned sequentially with detergent, deionized water and acetone, each step for 30 min, then dried with nitrogen gas and finally treated in a UV-ozone oven for 30 min. After passing through a 0.45 μm PVDF filter, the PEDOT:PSS solution (Baytron P VP AI 4083) was spin-coated onto the treated ITO substrates at 5000 rpm for 30 s and heated at 150 °C for 15 min in air. Then the substrates were transferred to a N_2-filled glovebox where $CH_3NH_3PbI_3$ (1 M solution in DMF) was spin-coated on top of the PEDOT:PSS coated substrates at 800 rpm for 10 s and at 4000 rpm for 25 s. 80 μL of toluene were added 5 s after the second step and then the devices were annealed at 70 °C for 60 min (a pure perovskite film was observed by XRD characterization, Figure S20). The fullerene derivatives dissolved in chlorobenzene (20 mg/mL) were spin-coated onto the $CH_3NH_3PbI_3$ layer at 5000 rpm for 30 s. Finally, Al

electrodes (100 nm) were deposited by thermal evaporation under a pressure of 1×10^{-6} Torr through a shadow mask. The active area of the fabricated devices was 6 mm^2. The Al electrodes were encapsulated with a UV-curable epoxy resin and a glass slide before testing. Stability studies were conducted on unencapsulated devices.

Results and discussion

The thiophene-based C_{60} fullerene derivatives **10–13** were synthesized as illustrated in scheme 1. Thiophene groups were selected not only to induce solubility, but also for their ability to passivate the perovskite crystals through sulfur-under-coordinated Pb^{+2} interactions (S···Pb), as theoretically and experimentally reported.[18, 23, 24] Considering that the CN group can increase the ε_r of fullerenes (from ~3 up to ~5)[21] it was introduced with the aim to polarize and increase the ε_r of the thiophene-based fullerenes. Finally, compounds **10–13** were synthesized via Bingel reactions that yield only [6,6]-isomers at room temperature, in good yields, and in short reaction times (see experimental section for details), compared to the synthesis of the widely used $PC_{61}BM$ via the tosylhydrazone route developed by Hummelen *et al.*, which leads to a mixture of isomers resulting from [5,6]-opened and [6,6]-closed additions, low yields, and long reaction times.[25]

The chemical structures of compounds **6–13** were confirmed by MALDI-TOF-MS, ^{1}H- and ^{13}C-NMR spectroscopy and UV-vis absorption (see supporting information, Figures S1-S12).

The electrochemical properties of compounds **10–13** were measured by CV on a glassy carbon electrode with *o*-DCB as the solvent and *n*-Bu_4NPF_6 as the supporting electrolyte. The onset of the first reduction potentials are shown in table 1. Very similar reduction potentials were observed for compounds **10–13** and $PC_{61}BM$,[26] as well as at least two well-defined and quasireversible redox waves (Figure S13). The LUMO energy levels of compounds **10–13** were calculated from their onset reduction potentials (E_{red}^{on}) using the formula: $\mathrm{LUMO} = -\mathrm{e}(E_{red}^{on} + 4.80)$ (eV).[27] The LUMO levels of compounds **10–13** are all estimated to be −3.88, −3.88, −3.88 and −3.86 eV, respectively. The HOMO energy levels of compounds **10–13** were calculated from their UV-absorption onset (E_g) (Figure S14) using the formula: HOMO = −e (LUMO − E_g) (eV). These results show that the LUMO/HOMO levels of compounds **10–13** are not affected by the presence of thiophene, CN or Br groups (Table 1).

The ε_r of the ETM plays an important role in preventing electron-hole recombinations in PSCs.[20, 28] It has been proven that ε_r is inversely proportional to the recombination ratio (r_c), as shown in equation 1.[20]

$$r_c = \frac{q^2}{4\pi\varepsilon_0\varepsilon_r kT} \quad (1)$$

where q, T, ε_0 and ε_r are the elementary charge, temperature, vacuum permittivity and the dielectric constant of the ETM, respectively.

Electrochemical impedance (EIS) was performed to measure the ε_r of the fullerene derivatives **10–13** and $PC_{61}BM$. The dependence of ε_r of **10–13** vs frequency (10 Hz - 0.1 MHz) is shown in figure 1a. Compounds **10**, **11** and **13** exhibit similar ε_r than that of $PC_{61}BM$ (around 3.9), but compound **12**, due to the presence of the CN group, exhibits a larger dipole moment than those of compounds **10**, **11**, **13** and $PC_{61}BM$ (Table 2). It is known that fullerenes functionalized with CN groups exhibit increased ε_r values by up to 26%.[21]

The electron mobility (μ_e) of fullerenes is also a very important parameter for their application as ETMs in PSCs.[15] The μ_e values of all fullerenes were measured using the space charge limit current (SCLC) method,[29] and using the dark *J-V* curves of electron-only devices with the configuration of ITO/Al/ETM/Al (Figure 1b). As listed in table 2, the μ_e of compounds **10–13** and $PC_{61}BM$ were determined to be 1.32×10^{-4}, 4.58×10^{-4}, 7.68×10^{-4}, 6.21×10^{-4} and 3.34×10^{-4} $cm^2\ V^{-1}\ s^{-1}$, respectively. These results show that the μ_e values of compounds **10–13** were not considerable affected by the presence of the thiophene, CN or Br groups.

The ability of compounds **10–13** to work as ETMs was tested by fabricating PSCs as schematically represented in figure 2a and described in detail in the experimental section. Figure 2b and 2c are top- and cross section SEM images of the perovskite film and PSC, respectively. The top-view image (Figure 2b) shows a homogeneous perovskite layer with large crystalline grains (~400 nm) and without apparent pinholes. Figure 2c shows the cross-section image of the PSC, where the perovskite layer adjacent to the HTL and ETL is clearly distinguished. Device performance variations are the result of the different fullerene derivative layers since all the PSCs were fabricated under identical conditions.

Figure 3b shows the *J-V* curves of the PSCs fabricated using compounds **10–13** and $PC_{61}BM$ as the ETMs. The control device based on $PC_{61}BM$ showed a performance with a J_{sc} of 21.10 mA/cm^2, a V_{oc} of 0.91 V, a fill factor (FF) of 0.82%, and a PCE of 15.11±0.6%. In contrast, devices based on compounds **10–13** showed significantly improved overall performances with average PCEs of 15.51±0.5%, 16.61±0.6%, 17.36±0.4% and 16.35±0.7%, respectively. The higher performance obtained from devices based on **12** (J_{sc} = 22.30, V_{oc} = 0.96, FF = 0.83% and PCE = 17.77%) results from the synergistic combination of specific surface interactions and higher ε_r value, which inhibit charge recombination and enhance charge collection.[15, 20, 30] The main photovoltaic characteristics are summarized in table 3. PSCs based on the fullerene derivatives showed negligible hysteretic behavior (Figures S15a-e). Device performance reproducibilities are calculated from the PCE distributions measured for 48 independent cells (Figure 3c). From figure 3d, it is clear that the EQE of the PSCs based on **12** are noticeably higher across the entire photoresponse range. The integrated photocurrent densities based on EQE measurements (Figure 3d) are consistent with those from *J-V* measurements (Table 3). The improved device performance was attributed to the better passivation ability of compounds **10–13**, because of specific interactions between the functional groups from the fullerene and the perovskite layer.

Figure 4 shows the Fourier transform infrared (FTIR) spectra of the perovskite, compound **12** and perovskite/**12** films. Clearly for the perovskite/**12** film the stretching bands at 2228 cm^{-1} (CN) and 1735 cm^{-1} (CO) are shifted and decreased in intensity, indicating the interaction between the fullerene and the perovskite layer, a similar trend was observed for the CO stretching band of compounds **10**, **11**, **13** and $PC_{61}BM$ (Figures S16-S18).

To probe the passivation ability of compounds **10–13** and the control $PC_{61}BM$ when deposited on the perovskite, we studied the photoluminescence (PL and TR-PL) of the photoactive layer (perovskite) with and without fullerenes. A significant PL quenching effect was observed for the perovskite layer coated with fullerenes **10–13** and $PC_{61}BM$ (Figure 5a). Compound **12** has a higher passivation ability than the other fullerenes, resulting in a more pronounced inhibition of the electron-hole recombination processes.[31].

Figure 5b shows the TR-PL decay measurements, monitoring the emission peak of the different fullerene derivative coated perovskite layers as a function of time. The pristine perovskite layer exhibits a PL lifetime of about 48.6 ns whereas perovskite/**10**, perovskite/**11**, perovskite/**12**, perovskite/**13**, and perovskite/$PC_{61}BM$, exhibit PL lifetimes of 47.9, 46.7, 45.1, 47.8 and 47.9 ns, respectively. Faster decays are measured for the samples coated with the fullerenes, which shows that the charge transfer processes are much faster than the charge recombination process in the perovskite layer.[31] The PL decay times are consistent with the observed PL quenching effect, suggesting that compound **12** has a better ability to suppress electron-hole recombination.

To further investigate the electrical and charge transport properties at the perovskite/fullerene interface, EIS was performed for PSCs based on compounds **10–13** and $PC_{61}BM$ (Figure 5c). The equivalent circuit used to fit the Nyquist plots is illustrated in figure 5c, the series resistance (R_s) corresponds to the resistance of the two electrodes, the charge-transport resistance (R_{ct}) and the recombination resistance (R_{rec}) correspond to the resistances at the fullerene/perovskite interfaces as extensively reported elsewhere.[32–34] As shown in figure 5c, PSCs based on **12** display a lower R_{ct} and larger R_{rec} values than devices based on **10**, **11**, **13** and $PC_{61}BM$ and considering that all the fullerenes have similar electron mobility and HOMO/LUMO energy values, the PCE improvement for devices based on **12** must result from improved interfacial contact and charge transfer between the perovskite and the compound **12**. These results demonstrate that electron extraction is more efficient at the perovskite/**12** interface than that for perovskite/**10**, perovskite/**11**, perovskite/**13** and perovskite/$PC_{61}BM$. In addition, a large R_{rec} was found when using compound **12**, which means that unfavourable recombination events occur at the perovskite/**12** interface. These results are also consistent with the higher PL quenching observed for perovskite/**12** films, which provide a rational explanation for the higher J_{sc} values.

The long term-device stabilities for PSCs were evaluated under ~20% humidity in air at room temperature without encapsulation for seven days (without continuous illumination). Figure 5d, shows the normalized PCEs against time. After seven days of periodic measurements, devices based on $PC_{61}BM$ lost 70% of their initial PCE. In contrast, devices based on compounds **10–13** lost less than 15% of their initial PCE under the same conditions.

Conclusions

In this work, new C_{60} fullerene derivatives functionalized with thiophene moieties as well as with electron donating or electron withdrawing groups bromine (Br) or cyano (CN), respectively, were synthesized via Bingel reactions and used as the ETMs in PSCs. We systematically studied the effect of the new fullerenes on PSCs performances by SCLC, FTIR, PL, TRPL, and EIS. The photoconversion efficiencies of PSCs based on compounds **10–13** were higher than those of devices based on $PC_{61}BM$, which can be associated with the better passivation ability, due to specific interactions between S···Pb atoms. The best photovoltaic performance was achieved for devices based on compound **12** (cyano derivative), likely due the synergistic effect of its higher ε_r, lower interfacial resistance and specific interactions between the carbonyl and cyano groups of the fullerene and the perovskite layer as determined from EIS and FTIR, respectively. These results show the importance of designing and synthesizing new fullerenes for their use in efficient PSCs.

Supplementary Material

Refer to Web version on PubMed Central for supplementary material.

Acknowledgements

Authors thank the US National Science Foundation (NSF) for generous support of this work under the NSF-PREM program (DMR 1205302), CHE-1408865 (to L.E.) and 1401188 (to F. D.). The Robert A. Welch Foundation is also gratefully acknowledged for an endowed chair to L. E. (Grant AH-0033). Research reported in this paper was supported by the National Institute of General Medical Sciences of the National Institutes of Health under linked Award Numbers RL5GM118969, TL4GM118971, and UL1GM118970. The content is solely the responsibility of the authors and does not necessarily represent the official views of the National Institutes of Health.

References

1. NREL, Best Research-Cell Efficiencies, https://www.nrel.gov/pv/assets/images/efficiency-chart.png, (accessed April, 2018).
2. Hu X, Huang Z, Zhou X, Li P, Wang Y, Huang Z, Su M, Ren W, Li F, Li M, Chen Y and Song Y Adv. Mater 2017, 29, 1703236.
3. Wang Y-C, Li X, Zhu L, Liu X, Zhang W and Fang J Adv. Energy Mater 2017, 7, 1701144.
4. Ghosh BK, Weoi CNJ, Islam A and Ghosh SK Renew. Sustainable Energy Rev 2018, 82, 1990–2004.
5. Bush KA, Palmstrom AF, Yu ZJ, Boccard M, Cheacharoen R, Mailoa JP, McMeekin DP, Hoye RLZ, Bailie CD, Leijtens T, Peters IM, Minichetti MC, Rolston N, Prasanna R, Sofia S, Harwood D, Ma W, Moghadam F, Snaith HJ, Buonassisi T, Holman ZC, Bent SF and McGehee MD Nat. Energy 2017, 2, 17009.
6. Castro E, Murillo J, Fernandez-Delgado O and Echegoyen L J. Mater. Chem. C 2018, 6, 2635–2651.
7. Nie W, Tsai H, Asadpour R, Blancon J-C, Neukirch AJ, Gupta G, Crochet JJ, Chhowalla M, Tretiak S, Alam MA, Wang H-L and Mohite AD Science 2015, 347, 522–525. [PubMed: 25635093]
8. Zheng X, Chen B, Dai J, Fang Y, Bai Y, Lin Y, Wei H, Zeng Xiao C. and Huang J Nat. Energy 2017, 2, 17102.
9. Castro E, Zavala G, Seetharaman S, D'Souza F and Echegoyen L J. Mater. Chem. A 2017, 5, 19485–19490.
10. Tian C, Castro E, Wang T, Betancourt-Solis G, Rodriguez G and Echegoyen L ACS Appl. Mater. Interfaces 2016, 8, 31426–31432. [PubMed: 27766845]
11. Chiang C-H, Nazeeruddin MK, Grätzel M and Wu C-G Energy Environ. Sci 2017, 10, 808–817.

12. Groeneveld BGHM, Najafi M, Steensma B, Adjokatse S, Fang H-H, Jahani F, Qiu L, Brink G. H. t., Hummelen JC and Loi MA APL Mater 2017, 5, 076103.
13. Tian C, Kochiss K, Castro E, Betancourt-Solis G, Han H and Echegoyen L Mater J Chem. A 2017, 5, 7326–7332.
14. Dong H, Wu Z, Xia B, Xi J, Yuan F, Ning S, Xiao L and Hou X Chem. Commun 2015, 51, 8986–8989.
15. Fang Y, Bi C, Wang D and Huang J ACS Energy Lett 2017, 2, 782–794.
16. Gatti T, Menna E, Meneghetti M, Maggini M, Petrozza A and Lamberti F Nano Energy 2017.
17. Deng L-L, Xie S-Y and Gao F Adv. Electron. Mater 2017, 1700435.
18. Noel NK, Abate A, Stranks SD, Parrott ES, Burlakov VM, Goriely A and Snaith HJ ACS Nano 2014, 8, 9815–9821. [PubMed: 25171692]
19. Xu J, Buin A, Ip AH, Li W, Voznyy O, Comin R, Yuan M, Jeon S, Ning Z, McDowell JJ, Kanjanaboos P, Sun J-P, Lan X, Quan LN, Kim DH, Hill IG, Maksymovych P and Sargent EH Nat. Commun 2015, 6, 7081. [PubMed: 25953105]
20. Shao S, Abdu-Aguye M, Qiu L, Lai L-H, Liu J, Adjokatse S, Jahani F, Kamminga ME, ten Brink GH, Palstra TTM, Kooi BJ, Hummelen JC and Antonietta Loi M Energy Environ. Sci 2016, 9, 2444–2452.
21. Zhang S, Zhang Z, Liu J and Wang L Adv. Funct. Mater 2016, 26, 6107–6113.
22. Jahani F, Torabi S, Chiechi RC, Koster LJA and Hummelen JC Chem. Commun 2014, 50, 10645–10647.
23. Kollek T, Wurmbrand D, Birkhold ST, Zimmermann E, Kalb J, Schmidt-Mende L and Polarz S ACS Appl. Mater. Inter 2017, 9, 1077–1085.
24. Zhang L, Yu F, Chen L and Li J Appl. Surf. Sci 2018, 443, 176–183.
25. Hummelen JC, Knight BW, Lepeq F, Wudl F, Yao J and Wilkins CL J. Org. Chem 1995, 60, 532–538.
26. Tian C, Castro E, Betancourt-Solis G, Nan Z-A, Fernandez-Delgado O, Jankuru S and Echegoyen L New J. Chem 2018, 42, 2896–2902.
27. Sun QJ, Wang HQ, Yang CH and Li YF J. Mater. Chem 2003, 13, 800–806.
28. Shao S, Liu J, Fang H-H, Qiu L, ten Brink GH, Hummelen JC, Koster LJA and Loi MA Adv. Energy Mater 2017, 1701305.
29. Murgatroyd PN J. Phys. D: Appl. Phys 1970, 3, 151.
30. Jiang Y, Li J, Xiong S, Jiang F, Liu T, Qin F, Hu L and Zhou Y J. Mater. Chem. A 2017, 5, 17632–17639.
31. Liang P-W, Liao C-Y, Chueh C-C, Zuo F, Williams ST, Xin X-K, Lin J and Jen AKY Adv. Mater 2014, 26, 3748–3754. [PubMed: 24634141]
32. Liu D, Yang J and Kelly TL J. Am. Chem. Soc 2014, 136, 17116–17122. [PubMed: 25405271]
33. Dualeh A, Moehl T, Tétreault N, Teuscher J, Gao P, Nazeeruddin MK and Grätzel M ACS nano 2013, 8, 362–373. [PubMed: 24341597]
34. Pitarch-Tena D, Ngo TT, Vallés-Pelarda M, Pauporté T and Mora-Seró I ACS Energy Lett 2018, 3, 1044–1048.

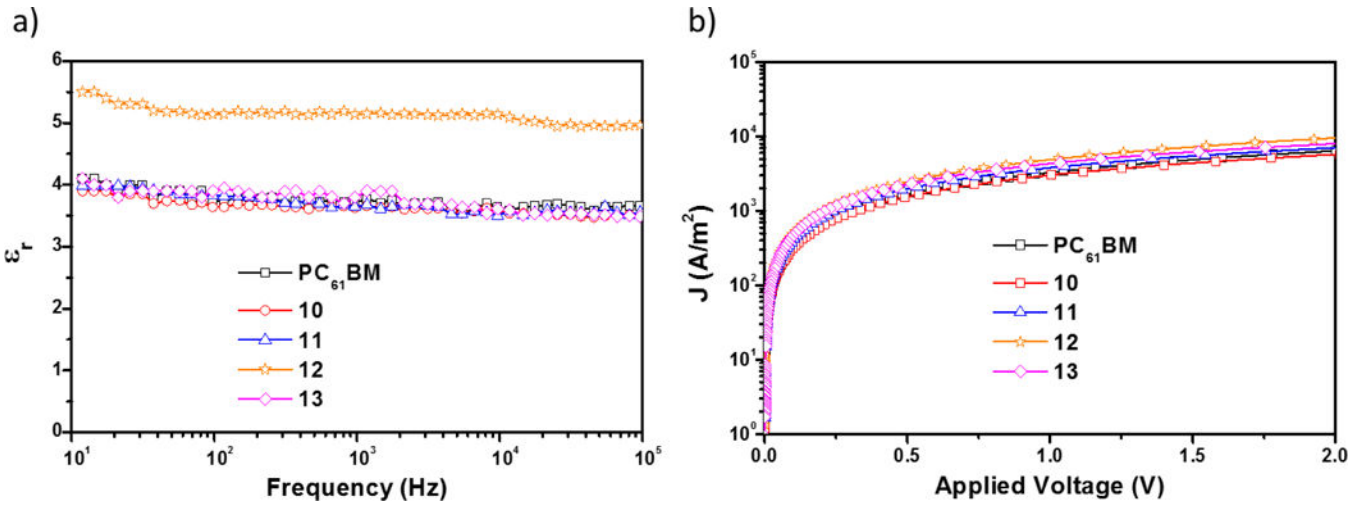

Figure 1.

a) dielectric constant vs frequency and b) electron mobility of the fullerene derivatives **10–13** and $PC_{61}BM$.

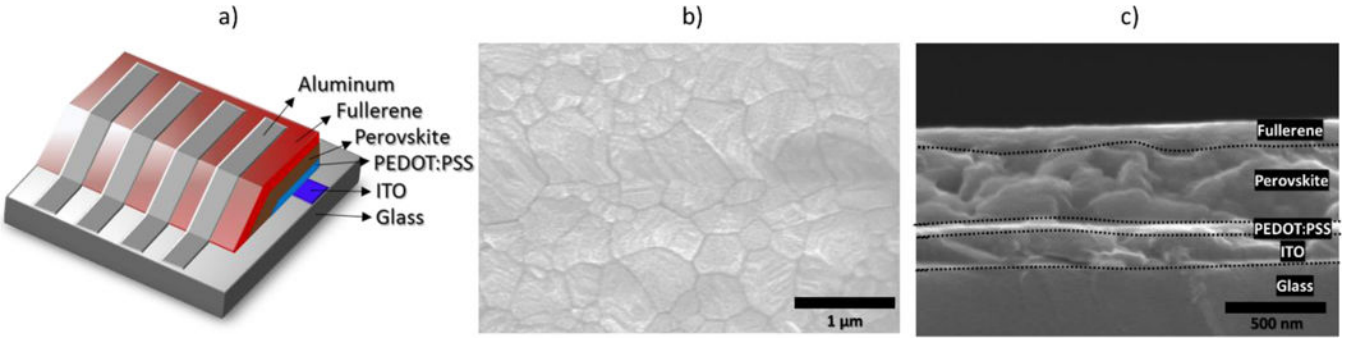

Figure 2.

(a) representation of the PSCs, (b) top-view SEM image of the perovskite film, and (c) cross-section SEM image of the device (ITO/PEDOT:PSS/perovskite/fullerene).

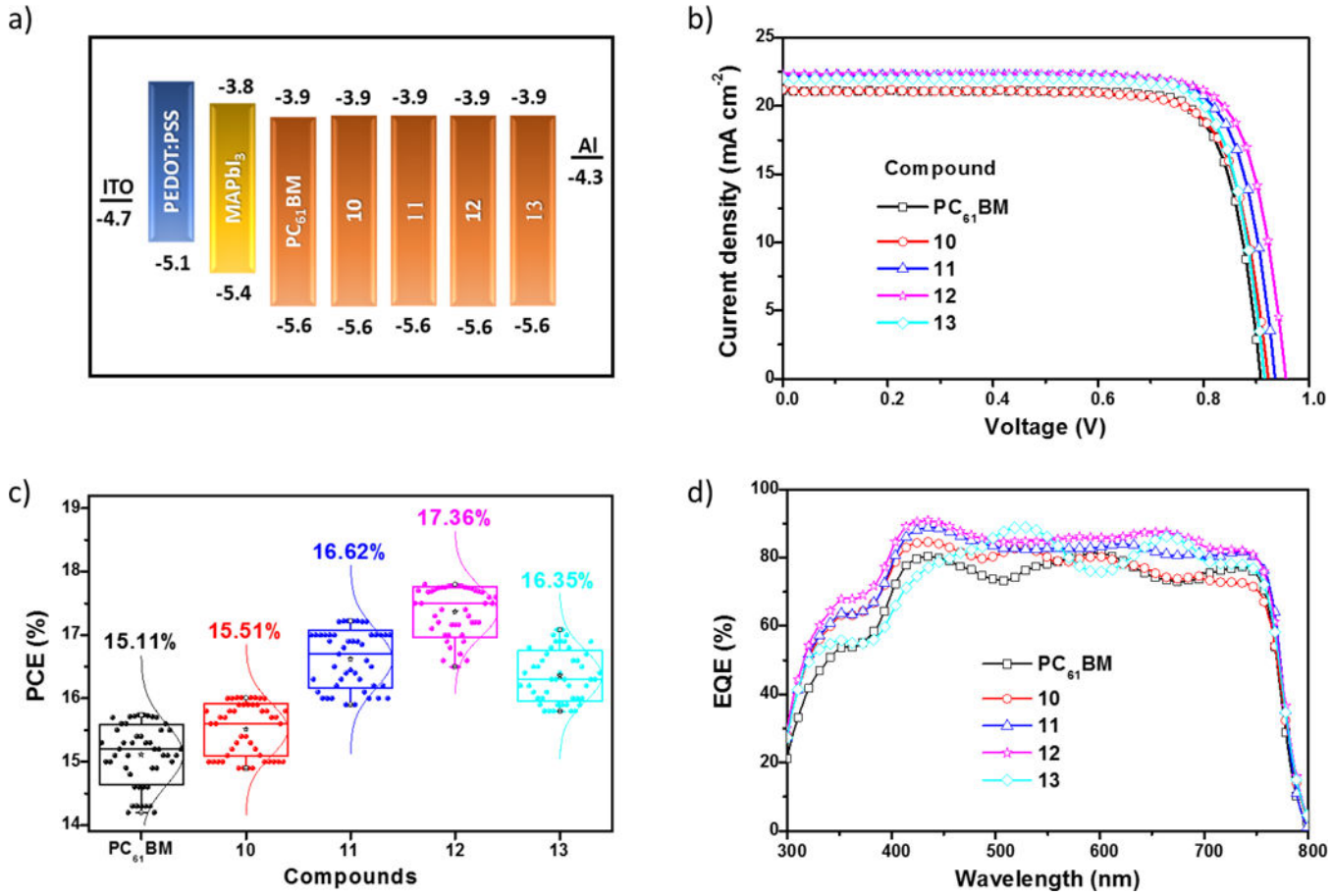

Figure 3.

a) Schematic illustration of the estimated HOMO and LUMO energy levels, calculated from CV and UV-vis. b) *J-V* curves under 1 sun illumination (100 mW/cm^2) in forward voltage scans. c) The PCE histograms measured for 48 independent cells. d) EQE spectra for the PSCs fabricated using compounds **10–13** and $PC_{61}BM$ as the ETMs.

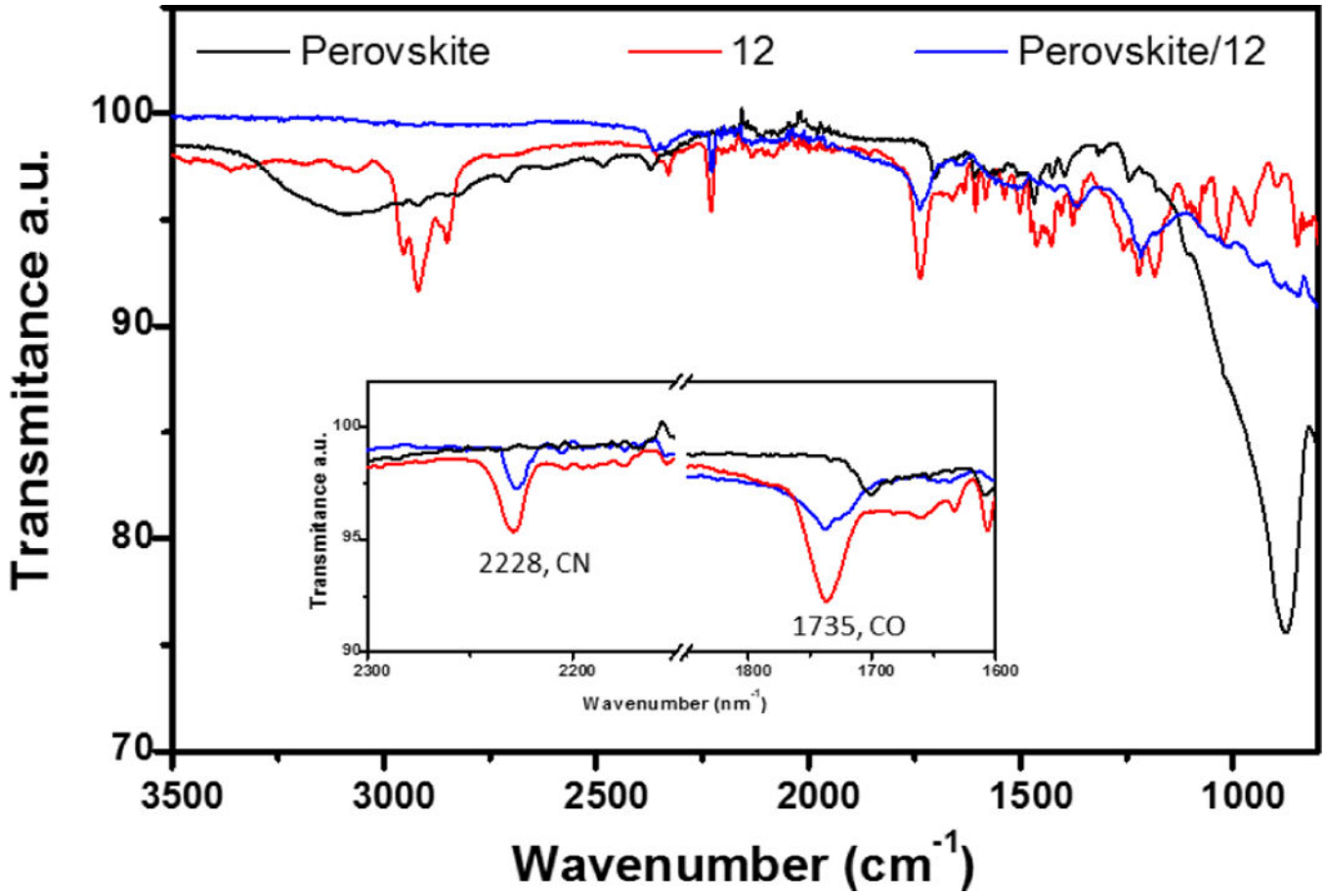

Figure 4.
FTIR spectra of perovskite, compound **12** and the perovskite/**12** films.

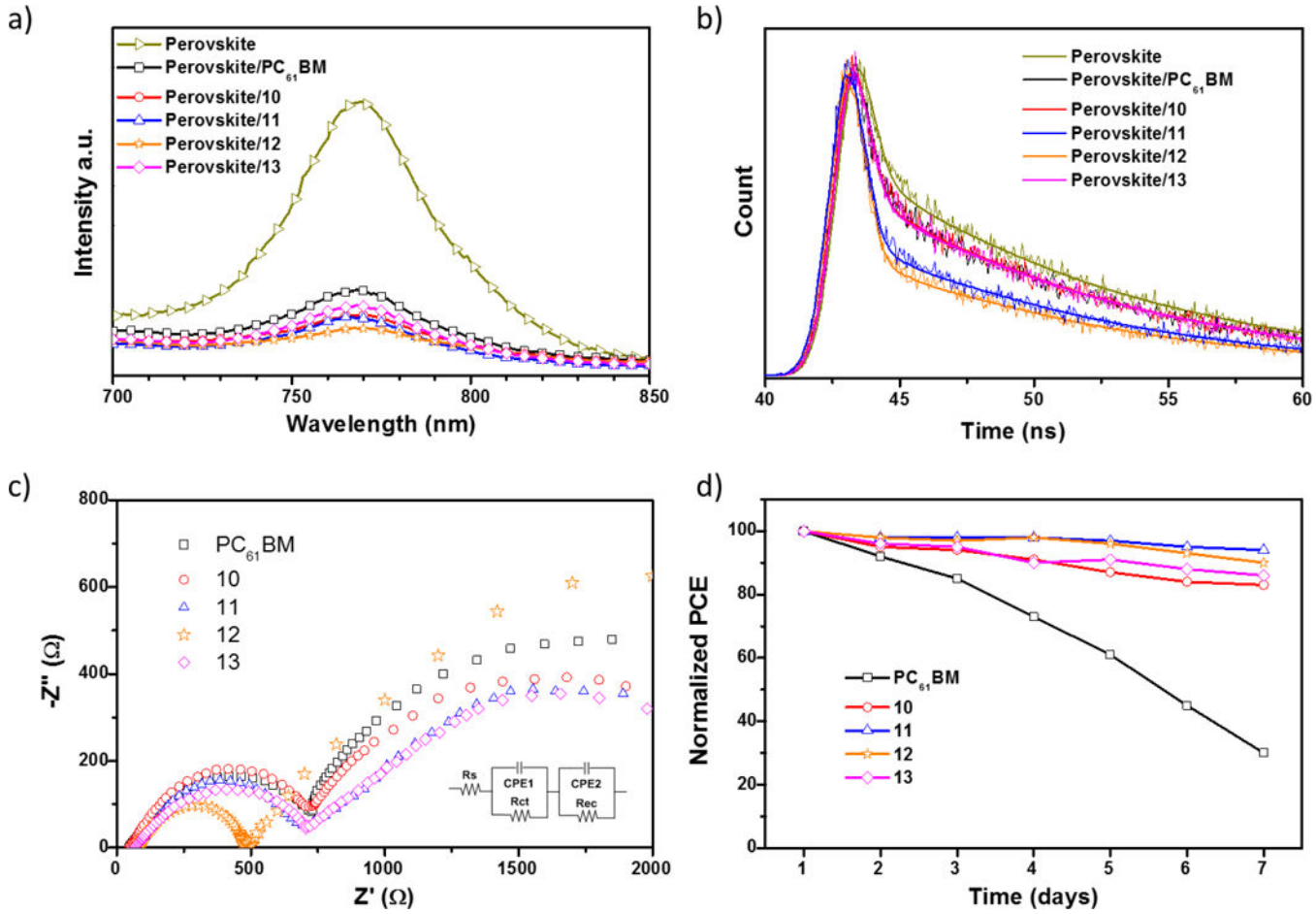

Figure 5.

a) Steady-state PL spectra of the perovskite and perovskite/ETM films. b) TR-PL spectra of the perovskite and perovskite/ETM films. c) Nyquist plots of the PSCs based on compounds **10–13** and $PC_{61}BM$ as the ETMs. d) Normalized PCEs of PSCs measured as a function of time in ~20% humidity at room temperature.

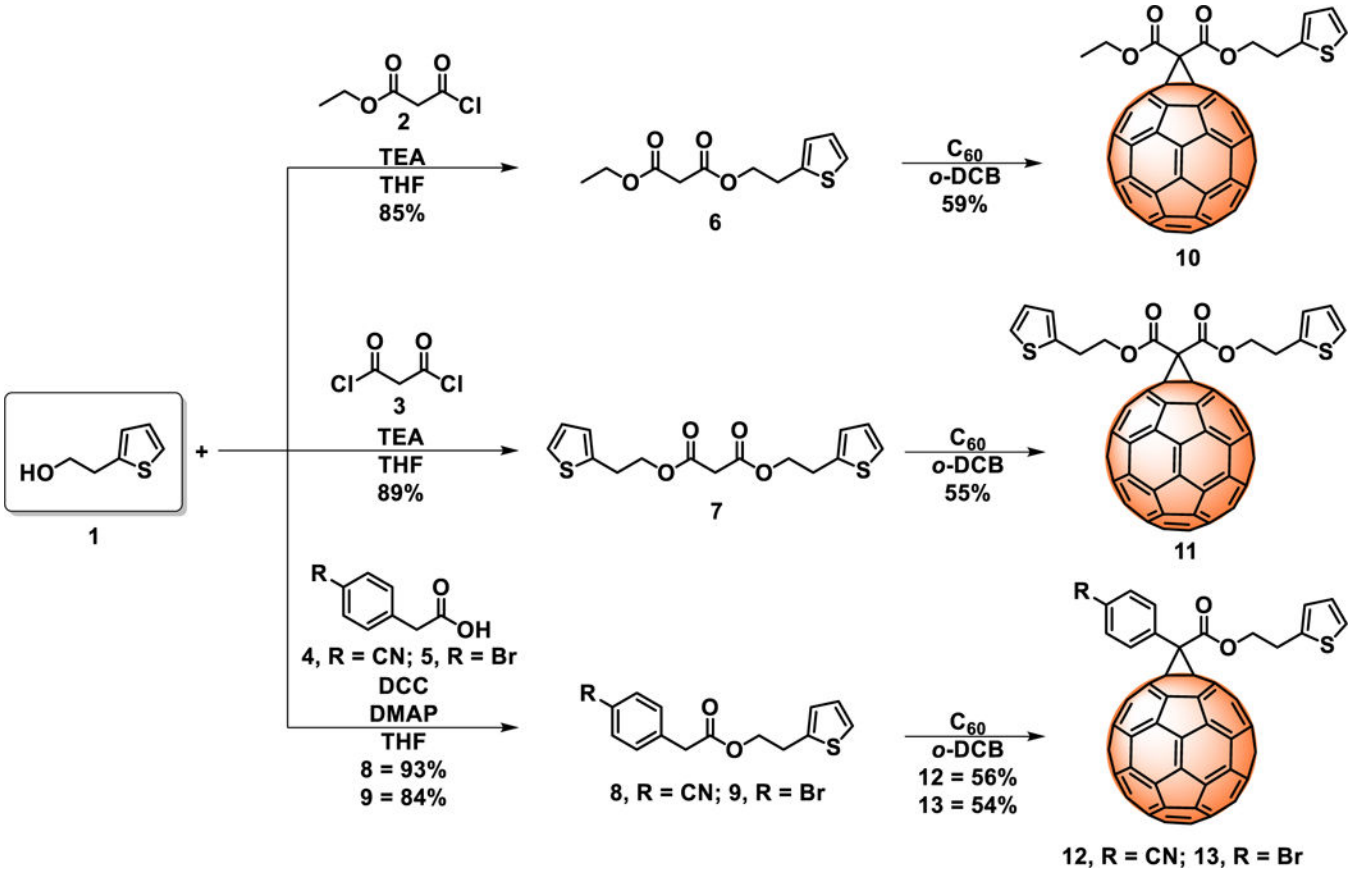

Scheme 1.

Synthesis of the thiophene-based C_{60} fullerene derivatives **10–13**.

Table 1.

Optical bandgap, onset reduction and LUMO/HOMO energy levels of $PC_{61}BM$ and **10–13**.

Compound	λ_{abs} (nm)	E_g (eV)	E^{on}_{red} (V)	LUMO (eV)	HOMO (eV)
$PC_{61}BM$ *	718	1.73	0.90	−3.90	−5.63
10	709	1.75	0.92	−3.88	−5.63
11	712	1.74	0.92	−3.88	−5.62
12	707	1.75	0.92	−3.88	−5.63
13	711	1.74	0.94	−3.86	−5.60

* LUMO/HOMO values were taken from the literature.[26]

Table 2.

Dielectric constant and electron mobility of the fullerene derivatives **10–13** and $PC_{61}BM$.

Compound	ε_r	μ_e ($cm^2\ V^{-1}\ s^{-1}$)
$PC_{61}BM$	3.8 ± 3	3.34×10^{-4}
10	3.6 ± 3	1.32×10^{-4}
11	3.7 ± 3	4.58×10^{-4}
12	5.2 ± 3	7.68×10^{-4}
13	3.7 ± 3	6.21×10^{-4}

Table 3.

Summary of device performance. The calculated J_{SC} values were obtained from the EQE curves. Values in parentheses represent the best PCEs measured.

Compound	Calculated J_{sc} (mA/cm^2)	J_{sc} (mA/cm^2)	V_{oc} (V)	FF (%)	PCE (%)
$PC_{61}BM$	21.03	21.10	0.91	0.82	15.11±0.6 (15.74)
10	20.85	21.00	0.93	0.82	15.51±0.5 (16.01)
11	21.78	22.10	0.94	0.83	16.61±0.6 (17.22)
12	22.19	22.30	0.96	0.83	17.36±0.4 (17.77)
13	22.04	22.10	0.92	0.84	16.35±0.7 (17.08)